

Modulation of the proteoglycan receptor PTP σ promotes recovery after spinal cord injury

Bradley T. Lang¹, Jared M. Cregg¹, Marc A. DePaul¹, Amanda P. Tran¹, Kui Xu², Scott M. Dyck³, Kathryn M. Madalena¹, Benjamin P. Brown⁴, Yi-Lan Weng⁵, Shuxin Li⁶, Soheila Karimi-Abdolrezaee³, Sarah A. Busch¹, Yingjie Shen² & Jerry Silver¹

Contusive spinal cord injury leads to a variety of disabilities owing to limited neuronal regeneration and functional plasticity. It is well established that an upregulation of glial-derived chondroitin sulphate proteoglycans (CSPGs) within the glial scar and perineuronal net creates a barrier to axonal regrowth and sprouting^{1–5}. Protein tyrosine phosphatase σ (PTP σ), along with its sister phosphatase leucocyte common antigen-related (LAR) and the nogo receptors 1 and 3 (NgR), have recently been identified as receptors for the inhibitory glycosylated side chains of CSPGs^{6–8}. Here we find in rats that PTP σ has a critical role in converting growth cones into a dystrophic state by tightly stabilizing them within CSPG-rich substrates. We generated a membrane-permeable peptide mimetic of the PTP σ wedge domain that binds to PTP σ and relieves CSPG-mediated inhibition. Systemic delivery of this peptide over weeks restored substantial

serotonergic innervation to the spinal cord below the level of injury and facilitated functional recovery of both locomotor and urinary systems. Our results add a new layer of understanding to the critical role of PTP σ in mediating the growth-inhibited state of neurons due to CSPGs within the injured adult spinal cord.

Our laboratory has developed an *in vitro* model of the inhibitory extracellular matrix that forms after spinal cord injury (SCI), wherein adult sensory neurons form dystrophic endballs as they attempt to traverse an increasing gradient of CSPG⁹. Our previous studies focused on dystrophic growth cones stalled within the CSPG gradient that remained active as they recycled membrane^{9,10}. We now report that chronic exposure to CSPG can induce the development of a distinct over-adhered morphology with no forward motility (Fig. 1a–c and Supplementary Videos 1–3). Any newly formed growth cones rapidly involute into large

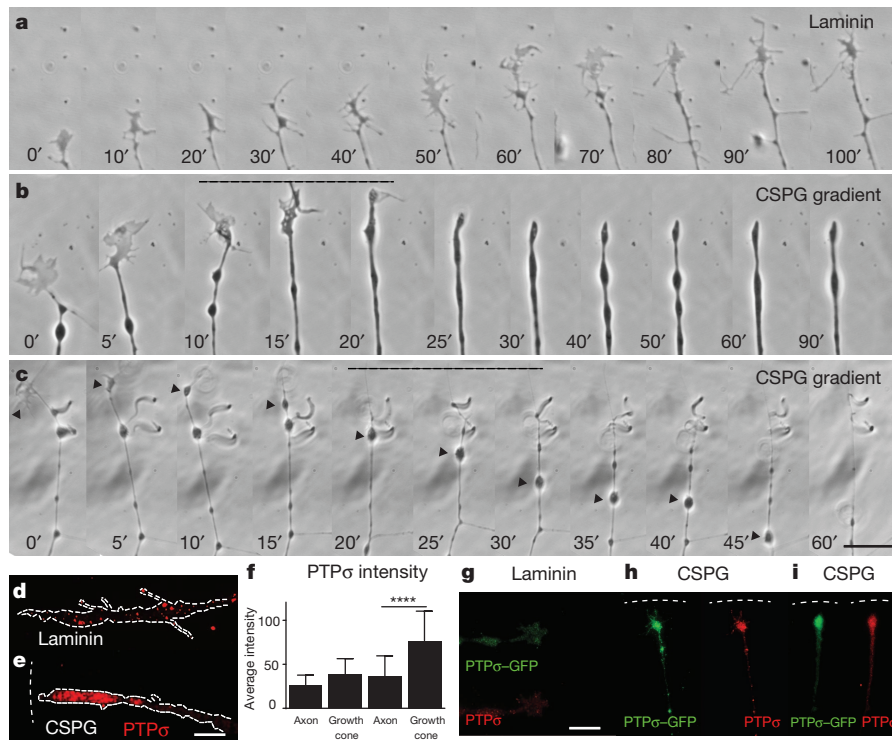


Figure 1 | Immobilization of growth cones within gradients of CSPG.

a–c, Time-lapse imaging in which the growth cones of adult sensory neurons are either motile upon a uniform substrate of laminin (**a**) or stabilizing within the gradient of proteoglycan (**b**, **c**). Arrowhead indicates absorbed growth cone. Timestamp indicates time in minutes. Scale bar, 20 μ m. See also Supplementary Videos 1–3. **d–j**, PTP σ staining in motile or stabilized growth

cones. $n = 16$ laminin, $n = 26$ CSPG for both treatments. Error bars show standard error of the mean (s.e.m.). **** $P < 0.0001$, $F = 19.9$, one-way analysis of variance (ANOVA), Tukey's post hoc test. **g–i**, Adult sensory neurons expressing a PTP σ -green fluorescent protein (GFP) plasmid. Dashed line indicates CSPG gradient.

¹Department of Neurosciences, Case Western Reserve University School of Medicine, Cleveland, Ohio 44106, USA. ²Center for Brain and Spinal Cord Repair, Department of Neuroscience, Wexner Medical Center at The Ohio State University, Columbus, Ohio 43210, USA. ³Regenerative Medicine Program and Department of Physiology, University of Manitoba, Winnipeg, Manitoba R3E 0J9, Canada. ⁴Baldwin Wallace University, Berea, Ohio 44017, USA. ⁵Institute for Cell Engineering, Johns Hopkins University School of Medicine, Baltimore, Maryland, 21205, USA. ⁶Shriners Hospital's Pediatric Research Center (Center for Neural Repair and Rehabilitation), Temple University School of Medicine, Philadelphia, Pennsylvania 19140, USA.

blebs, resulting in a beaded axon with one tip or multiple side branches, all terminating in small punctate adhesive contacts (Fig. 1c and Supplementary Video 3). This morphology is remarkably similar to that described in the early 20th century by Ramon y Cajal in the chronically injured cat spinal cord¹¹.

Interestingly, although PTP σ is evenly distributed in a punctate pattern within motile axons and growth cones, it becomes concentrated in dystrophic stabilized growth cones (Fig. 1d–i). We found similar elevations of LAR, but not NgRs (Extended Data Fig. 1a, b). In addition, we observed a large concentration of PTP σ in the lesion penumbra after SCI (Extended Data Fig. 1c, d). As PTP σ co-localizes with adhesion plaques and focal adhesions^{12,13}, we hypothesized that it had a critical role in growth cone immobilization and progression into a dystrophic state. Therefore, we sought to target PTP σ to relieve CSPG-mediated inhibition.

Upon analysing the structure of PTP σ and related phosphatases, we identified a highly conserved 24-amino-acid intracellular wedge domain (Fig. 2a and Extended Data Fig. 2a, b). As wedge domains are known to regulate downstream signalling through a variety of mechanisms^{7,14–16}, we designed intracellular sigma peptide (ISP), a novel peptide-mimetic of the PTP σ wedge with a TAT domain to facilitate membrane penetration (Fig. 2b).

ISP was able to bind to recombinant human PTP σ (Fig. 2c). In rodent brain and spinal cord lysates, ISP pulled down both immature full-length PTP σ and the mature functional complex (Fig. 2d–f)¹². In PTP σ -null mice, only a very minor signal was detected, which may reflect non-specific binding to PTP δ , the third LAR family member (Fig. 2d, e)¹⁷. No detectable binding was observed between ISP and other CSPG receptors such as LAR and NgRs (Extended Data Fig. 2e, f). Interestingly, a LAR wedge-domain peptide (ILP)¹⁴ was also capable of binding PTP σ , but less efficiently than ISP (Fig. 2d, f and Extended Data Fig. 2c, d).

We next asked whether ISP could release CSPG-mediated axonal inhibition *in vitro*. ISP treatment allowed adult sensory neurons to extend axons through a CSPG gradient in a dose-dependent manner to the same extent as pre-treatment with chondroitinase ABC (ChABC), which cleaves the glycosylated CSPG side chains and removes the PTP σ ligand (Fig. 2g–i)⁶. Time-lapse microscopy revealed that although growth cones treated with ISP were still transiently collapsed by CSPG, they continued to reform growth cones, allowing them to eventually cross the gradient (Fig. 2k and Supplementary Video 4). Additionally, both ISP and ChABC treatments were sufficient to convert already stabilized dystrophic growth cones into a motile state (data not shown). Interestingly, human ISP and the wedge domain peptides of PTP δ and LAR (IDP and ILP) demonstrated some efficacy, suggesting functional redundancy among LAR

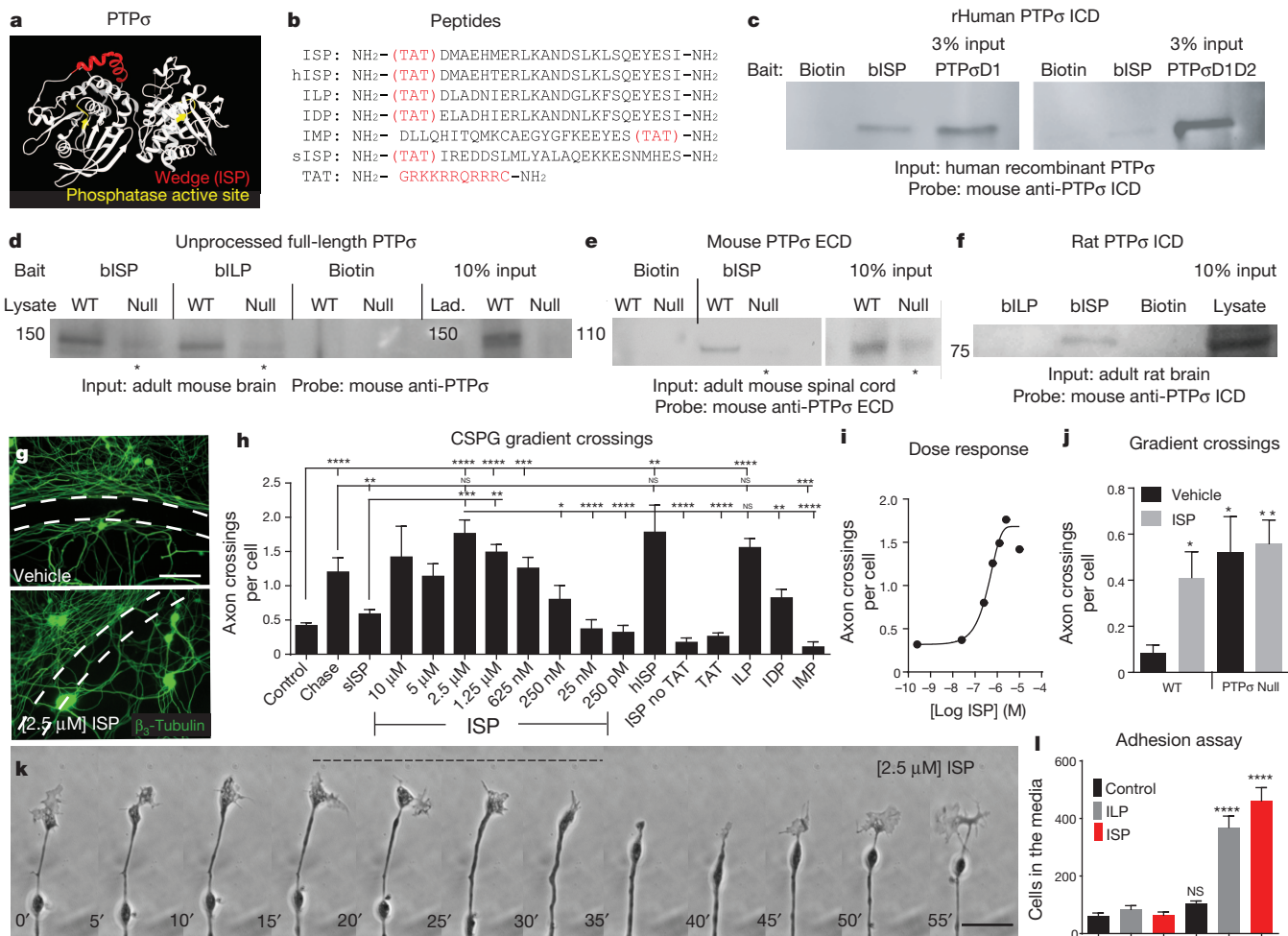


Figure 2 | Identification and characterization of ISP. **a**, PTP σ structure and wedge domain (red). **b**, Peptide sequences. **c–f**, Pulldown of human, rat and mouse PTP σ with biotinylated ISP (bISP). Asterisk indicates nonspecific recognition of PTP δ . ICD, intracellular domain; D1, PTP σ domain 1; D1D2, PTP σ domain 1–2; Lad, ladder (kilodaltons); r, recombinant; WT, wild type. Four repetitions. **g–i**, CSPG gradient crossing assay. Dashed lines indicate CSPG gradient. Scale bar, 50 μm; $n > 16$ gradients per group. hISP, human ISP; sISP, scrambled ISP. **j**, ISP treatment on PTP σ -null neurons

($n = 12$ per group, 3 repetitions). **k**, Time-lapse imaging of an adult sensory neuron growth cone after 2.5 μM ISP treatment (Supplementary Video 4). Timestamp indicates time in minutes. Scale bar, 20 μm. **l**, The number of neurons released from a CSPG-rich substrate after agitation ($n = 28$ vehicle/ILP, $n = 16$ ISP wells per group). Scale bar, 50 μm. Error bars show s.e.m. * $P < 0.05$, ** $P < 0.01$, *** $P < 0.001$, **** $P < 0.0001$, one-way ANOVA, Tukey's post hoc test. For additional sample size information, see Methods.

family wedge domains. The wedge domain of PTP μ (IMP), scrambled ISP, TAT alone, or ISP without TAT were ineffective (Fig. 2h).

Importantly, treatment of adult PTP σ -null sensory neurons with ISP did not further increase crossings (Fig. 2j)⁶. In addition, mature astrocytes, which have immunocytochemically undetectable PTP σ ¹⁸, were unable to traverse the CSPG gradient after ISP treatment (Extended Data Fig. 3a). However, PTP σ -expressing satellite glia were induced to cross successfully (Extended Data Fig. 3b). These results suggest specificity of ISP interactions through PTP σ .

ISP concentrations above the optimal dose for gradient crossing greatly reduced neuronal cell attachment, suggesting a reversal of the over-adhered phenotype. ISP treatment decreased interactions between the CSPG-rich substrate and PTP σ , allowing cells to detach in response to agitation (Fig. 2l and Extended Data Fig. 3c, d). This suggests that appropriate levels of adhesion are critical for regeneration across increasing concentrations of innately inhibitory CSPGs¹⁹.

The extracellular-signal-regulated kinase 1/2 (Erk1/2) cascade regulates a variety of processes, including axonal growth²⁰. Erk1/2 phosphorylation was decreased in neuronal cells grown on a CSPG-rich substrate and both ISP and ChABC were able to restore the phosphorylation

state of Erk1/2 to levels comparable to that on laminin-only substrates (Extended Data Fig. 4)²¹.

TAT-conjugated peptides are known to cross biological membranes, including the blood-brain barrier²². One hour after a single subcutaneous injection of fluorescein isothiocyanate (FITC)-conjugated ISP, we were able to visualize ISP in the intact nervous system (Extended Data Fig. 5a, b). Therefore, we chose a non-invasive systemic treatment paradigm using daily subcutaneous injections, avoiding complications associated with intraparenchymal delivery²³. Beginning 1 day after contusive SCI, rats were treated with ISP (11 µg per day), ILP (11 µg per day) or vehicle once daily for 7 consecutive weeks (Extended Data Fig. 5c–e).

SCI disrupts connections between the bladder and brainstem micturition control centre, leading to reduced void frequency and an accompanying increase in void volume (Extended Data Fig. 6a, b)²⁴. Twelve weeks after injury, ISP promoted a significant twofold increase in void frequency versus controls, along with a significant decrease in void volume (Fig. 3a–c and Extended Data Fig. 6c–h). We used urodynamics to assess whether this improvement was a result of physiologically normal bladder activity. Rats urinate by contracting the detrusor muscle, resulting in a rapid increase in bladder pressure while the external urethral sphincter

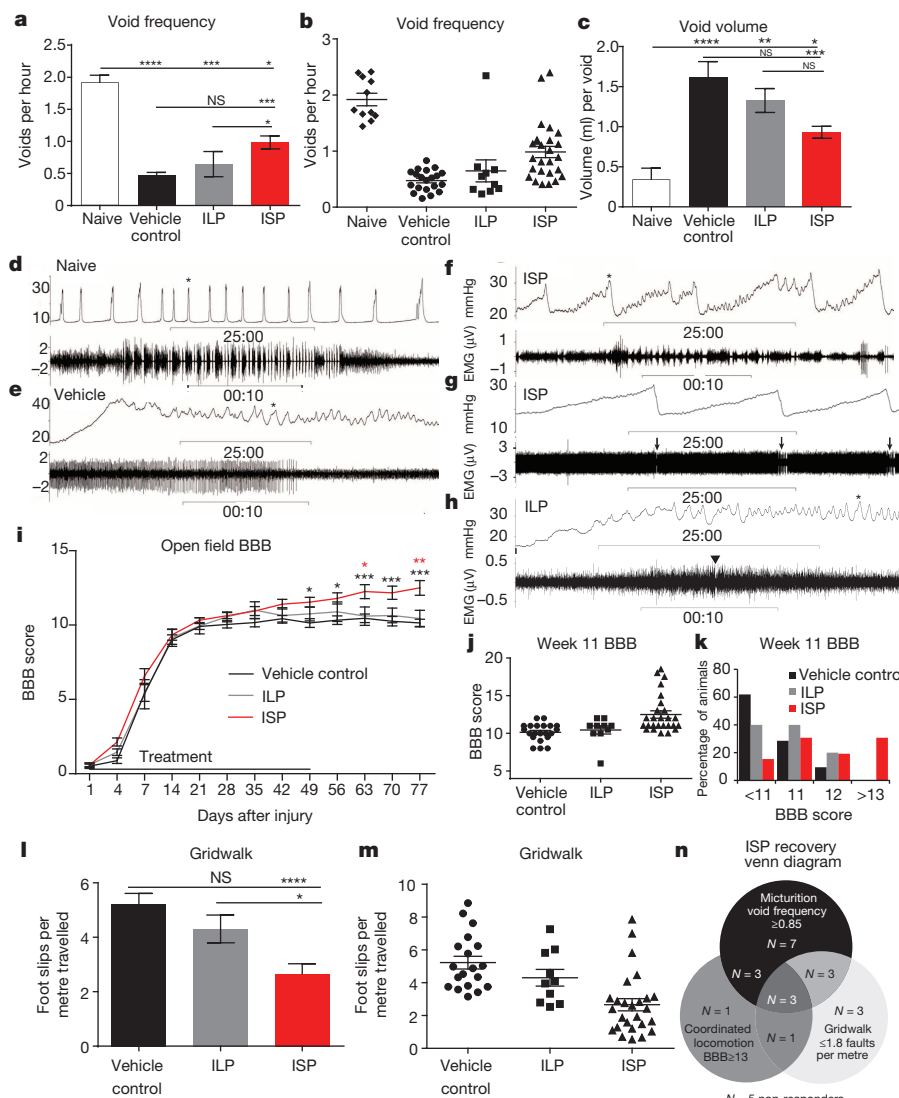


Figure 3 | Functional recovery after ISP treatment. **a–c.** Void frequency and average void volume at 12 weeks after SCI. **d–h.** Representative urodynamic recordings of detrusor activity (bladder pressure, top trace) and EUS activity (bottom trace). Arrows indicate synchronized phasic bursting; arrowhead indicates single burst. **i–k.** Locomotor recovery (BBB score) after treatment. **l–m.** Gridwalk test at 12 weeks after SCI. **n.** ISP functional recovery Venn diagram (21/26 ISP, 0/21 vehicle, 1/10 ILP). Error bars show s.e.m. *P < 0.05, **P < 0.01, ***P < 0.001, ****P < 0.0001, repeated measures two-way ANOVA, Tukey's post-hoc test (BBB); one-way ANOVA, Kruskal-Wallis post-hoc test (gridwalk and micturition). NS, not significant. Black indicates ISP versus control; red indicates ISP versus ILP.

SCI. **l, m.** Gridwalk test at 12 weeks after SCI. **n.** ISP functional recovery Venn diagram (21/26 ISP, 0/21 vehicle, 1/10 ILP). Error bars show s.e.m. *P < 0.05, **P < 0.01, ***P < 0.001, ****P < 0.0001, repeated measures two-way ANOVA, Tukey's post-hoc test (BBB); one-way ANOVA, Kruskal-Wallis post-hoc test (gridwalk and micturition). NS, not significant. Black indicates ISP versus control; red indicates ISP versus ILP.

(EUS) bursts phasically, expelling urine (Fig. 3d)²⁵. No vehicle- or ILP-treated animals displayed multiple coordinated bursts of the EUS during a void (Fig. 3e, h). Although the detrusor was still hyperactive, 10 of the 15 analysed ISP-treated animals recovered coordination between bladder contractions and EUS phasic bursting, suggesting reconnection of a functional circuit (Fig. 3f, g)²⁶.

We measured locomotor recovery using the Basso, Beattie and Bresnahan (BBB) scale and a gridwalk test²⁷. After SCI, vehicle- and ILP-treated animals recovered from hindlimb paralysis at day 1 to, on average, occasional weight bearing stepping at week 11 (Fig. 3i). ISP treatment resulted in a significant progressive recovery of locomotion, which began several weeks after injury (Fig. 3i). Thirty per cent of ISP-treated animals (versus zero vehicle/ILP-treated animals) demonstrated, at least, frequent coordinated stepping (BBB ≥ 13), with three rats achieving BBB scores ≥ 17.5 (Fig. 3j–k). Furthermore, ISP-treated animals made on average 58% fewer foot faults than control rats on the gridwalk test (Fig. 3l, m), suggesting recovery of sensorimotor coordination and balance. Importantly, aside from minor irritation at the injection site after multiple weeks of treatment, ISP did not induce neuropathic pain (Extended Data Fig. 7a, b).

Interestingly, no correlation between ISP-induced recovered behaviours was observed (Extended Data Fig. 7c–e). Using stringent threshold analyses, we determined that 21 of 26 ISP-treated animals recovered at least one behaviour, with 3 animals recovering all three (Fig. 3n). Further analyses demonstrated the degree to which responding animals benefited from treatment (Extended Data Fig. 7f–h). Taken together, this suggests that the re-acquisition of each behaviour is modular and not coincident, and may reflect anatomical differences in the pattern of axon re-innervation.

The behavioural results represent the average of five repetitions, each performed with newly synthesized peptide, blinded behavioural testers and a separate blinded treatment administrator. Although variability

existed, ISP increased functional recovery of each behaviour in all cohorts (Extended Data Fig. 8). In a final group of animals, urinary, but not locomotor behaviours, responded to increasing concentrations of ISP, with our maximum (44 µg per day) dose improving urination markedly in all rats (Extended Data Fig. 7g). Therefore, further optimization of the dose or administrative route of ISP may lead to additional functional improvements.

ISP treatment was not neuroprotective, as it did not lead to differences in lesion size or spared white matter (Fig. 4a, b). At the individual animal level, the variability in spared tissue correlated with functional recovery in vehicle-, but not ISP-treated rats (Extended Data Fig. 9).

Although regenerative pathways are difficult to examine after contusive SCI²⁸, we did not observe any lengthy regenerating biotinylated dextran amine (BDA)-labelled corticospinal tract fibres (data not shown). We focused further analysis on the serotonergic system (5HT) neurons, which express LAR family receptors and contribute to proper neuromodulatory tone in locomotion and micturition circuitry^{7,26,29,30}. Contusive SCI led to a marked decrease in descending 5HT-positive fibres caudal to the lesion (Fig. 4c, e, h). In animals exhibiting functional recovery after ISP treatment, we observed unusually shaped, densely sprouted territories of 5HT fibres below the level of the lesion (Fig. 4d, f, i–n). These patterns corresponded in part with neurofilament staining (Extended Data Fig. 10), but were not present in sections stained for GFAP, ED1 or 4',6-diamidino-2-phenylindole (DAPI), ensuring that the sharp edges of staining were not due to tissue folds. We speculate that physical constraints of the perineuronal net may confine fibres in these patterns. Their spatial variability, in conjunction with differences in tract sparing from animal to animal after contusion, could partially account for the disparity in behavioural recovery between animals.

Treatment with the 5HT receptor antagonist methysergide at 14 weeks after SCI significantly reduced locomotor and urinary function in ISP-treated, but not vehicle-treated animals (Fig. 4o, p)^{26,29}. This was most

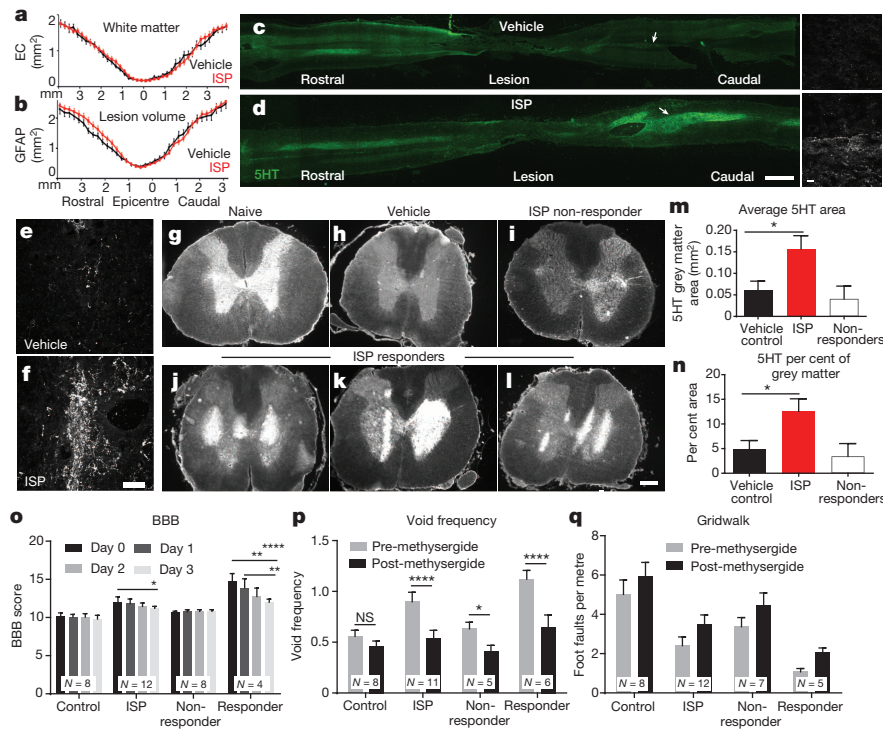


Figure 4 | Anatomical changes after ISP treatment. **a, b,** Average lesion size (GFAP) and spared white matter (eriochrome cyanine (EC) staining) after SCI. $n = 9\text{--}10$ vehicle, $n = 14$ ISP. **c, d,** 5HT intensity in representative longitudinal spinal cord sections. Insets reveal fibre density. Scale bar, 2 mm; inset, 20 μm . **e, f,** Representative confocal projections of caudal 5HT fibres at L1–L3. Scale bar, 20 μm . **g–l,** 5HT intensity across lumbar coronal sections. Scale bar, 500 μm . **m, n,** Average area and per cent coverage of 5HT. $n = 13$

vehicle, $n = 18$ ISP. $P < 0.05$, Student's t -test (two tailed). **o–q,** Behavioural response to methysergide at 14 weeks after SCI. ‘Responders’ are animals demonstrating functional recovery in each behaviour. $n = 8$ vehicle, $n = 11\text{--}12$ ISP. Error bars show s.e.m. * $P < 0.05$, ** $P < .01$, *** $P < 0.001$, two-way repeated measures ANOVA, Tukey's post-hoc test (BBB); one-way ANOVA, Kruskal–Wallis post hoc test (gridwalk and void frequency). NS, not significant.

evident in ISP responders, animals that regained function beyond recovery thresholds. However, behavioural improvements were not fully reverted to vehicle levels and gridwalk scores were only minimally affected (Fig. 4q), suggesting plasticity of other pathways outside the serotonergic system.

While CSPGs have largely been thought to act as repulsive components of the extracellular matrix, our results suggest that regenerating adult growth cones can become permanently immobilized by CSPG gradients. These observations highlight an initial cellular mechanism regulated by PTP σ that leads to the development of axonal dystrophy and the prevention of chronic regeneration and plasticity *in vivo*. Systemic modulation of PTP σ opens a new therapeutic avenue in non-invasive treatments for enhancing functional recovery after a variety of injuries or diseases in which proteoglycans inhibit the attempt of axons to regenerate or sprout.

Online Content Methods, along with any additional Extended Data display items and Source Data, are available in the online version of the paper; references unique to these sections appear only in the online paper.

Received 8 July; accepted 16 October 2014.

Published online 3 December 2014.

- Cregg, J. M. et al. Functional regeneration beyond the glial scar. *Exp. Neurol.* **253**, 197–207 (2014).
- Andrews, E. M., Richards, R. J., Yin, F. Q., Viapiano, M. S. & Jakeman, L. B. Alterations in chondroitin sulfate proteoglycan expression occur both at and far from the site of spinal contusion injury. *Exp. Neurol.* **235**, 174–187 (2012).
- Pizzorusso, T. et al. Reactivation of ocular dominance plasticity in the adult visual cortex. *Science* **298**, 1248–1251 (2002).
- Bradbury, E. J. et al. Chondroitinase ABC promotes functional recovery after spinal cord injury. *Nature* **416**, 636–640 (2002).
- Massey, J. M. et al. Chondroitinase ABC digestion of the perineuronal net promotes functional collateral sprouting in the cuneate nucleus after cervical spinal cord injury. *J. Neurosci.* **26**, 4406–4414 (2006).
- Shen, Y. et al. PTP σ is a receptor for chondroitin sulfate proteoglycan, an inhibitor of neural regeneration. *Science* **326**, 592–596 (2009).
- Fisher, D. et al. Leukocyte common antigen-related phosphatase is a functional receptor for chondroitin sulfate proteoglycan axon growth inhibitors. *J. Neurosci.* **31**, 14051–14066 (2011).
- Dickendesher, T. L. et al. NgR1 and NgR3 are receptors for chondroitin sulfate proteoglycans. *Nature Neurosci.* **15**, 703–712 (2012).
- Tom, V. J., Steinmetz, M. P., Miller, J. H., Doller, C. M. & Silver, J. Studies on the development and behavior of the dystrophic growth cone, the hallmark of regeneration failure, in an *in vitro* model of the glial scar and after spinal cord injury. *J. Neurosci.* **24**, 6531–6539 (2004).
- Busch, S. A., Horn, K. P., Silver, D. J. & Silver, J. Overcoming macrophage-mediated axonal dieback following CNS injury. *J. Neurosci.* **29**, 9967–9976 (2009).
- Cajal, S. R. Y. *Degeneration & Regeneration of the Nervous System* (Oxford Univ. Press, 1928).
- Aicher, B., Lerch, M. M., Muller, T., Schilling, J. & Ullrich, A. Cellular redistribution of protein tyrosine phosphatases LAR and PTP σ by inducible proteolytic processing. *J. Cell Biol.* **138**, 681–696 (1997).
- Serra-Pagès, C. et al. The LAR transmembrane protein tyrosine phosphatase and a coiled-coil LAR-interacting protein co-localize at focal adhesions. *EMBO J.* **14**, 2827–2838 (1995).
- Xie, Y. et al. Protein-tyrosine phosphatase (PTP) wedge domain peptides: a novel approach for inhibition of PTP function and augmentation of protein-tyrosine kinase function. *J. Biol. Chem.* **281**, 16482–16492 (2006).
- Jiang, G. et al. Dimerization inhibits the activity of receptor-like protein-tyrosine phosphatase- α . *Nature* **401**, 606–610 (1999).
- Barr, A. J. et al. Large-scale structural analysis of the classical human protein tyrosine phosphatome. *Cell* **136**, 352–363 (2009).
- Wallace, M. J., Fladd, C., Batt, J. & Rotin, D. The second catalytic domain of protein tyrosine phosphatase δ (PTP δ) binds to and inhibits the first catalytic domain of PTP σ . *Mol. Cell. Biol.* **18**, 2608–2616 (1998).
- Silver, D. J. et al. Chondroitin sulfate proteoglycans potently inhibit invasion and serve as a central organizer of the brain tumor microenvironment. *J. Neurosci.* **33**, 15603–15617 (2013).
- Lowery, L. A. & Van Vactor, D. The trip of the tip: understanding the growth cone machinery. *Nature Rev. Mol. Cell Biol.* **10**, 332–343 (2009).
- Polleux, F. & Snider, W. Initiating and growing an axon. *Cold Spring Harb. Perspect. Biol.* **2**, a001925 (2010).
- Sapieha, P. S. et al. Receptor protein tyrosine phosphatase sigma inhibits axon regrowth in the adult injured CNS. *Mol. Cell. Neurosci.* **28**, 625–635 (2005).
- Banks, W. A., Robinson, S. M. & Nath, A. Permeability of the blood–brain barrier to HIV-1 Tat. *Exp. Neurol.* **193**, 218–227 (2005).
- Jones, L. L. & Tuszyński, M. H. Chronic intrathecal infusions after spinal cord injury cause scarring and compression. *Microsc. Res. Tech.* **54**, 317–324 (2001).
- de Groat, W. C. et al. Mechanisms underlying the recovery of urinary bladder function following spinal cord injury. *J. Auton. Nerv. Syst.* **30** (suppl.), S71–S77 (1990).
- Pikov, V. & Wrathall, J. R. Coordination of the bladder detrusor and the external urethral sphincter in a rat model of spinal cord injury: effect of injury severity. *J. Neurosci.* **21**, 559–569 (2001).
- Lee, Y. S. et al. Nerve regeneration restores supraspinal control of bladder function after complete spinal cord injury. *J. Neurosci.* **33**, 10591–10606 (2013).
- Basso, D. M., Beattie, M. S. & Bresnahan, J. C. A sensitive and reliable locomotor rating scale for open field testing in rats. *J. Neurotrauma* **12**, 1–21 (1995).
- Tuszyński, M. H. & Steward, O. Concepts and methods for the study of axonal regeneration in the CNS. *Neuron* **74**, 777–791 (2012).
- Murray, K. C. et al. Recovery of motoneuron and locomotor function after spinal cord injury depends on constitutive activity in 5-HT2C receptors. *Nature Med.* **16**, 694–700 (2010).
- Xu, B. et al. Role of CSPG receptor LAR phosphatase in restricting axon regeneration after CNS injury. *Neurobiol. Dis.* **73C**, 36–48 (2014).

Supplementary Information is available in the online version of the paper.

Acknowledgements This work was supported by National Institute of Neurological Disorders and Stroke grant NS025713 (J.S.); the Case Western Reserve University Council to Advance Human Health; P. Jing, R. Senior and S. Poon; Unite to Fight Paralysis; The Brumagin Memorial Fund; Spinal Cord Injury Sucks; United Paralysis Foundation; and The Kaneko Family Fund. The authors thank J. Flanagan, M. Blackmore, A. Filous, S. Brady-Kalnay, R. Gardner and B. Habecker for their valuable discussion and input into the project.

Author Contributions B.T.L. performed all *in vitro* experiments, time-lapse microscopy, ISP treatments, immunohistochemistry and data quantification. B.T.L., J.M.C. and Y.L.W. designed the peptides. M.A.D. and A.T. performed all surgical procedures. B.T.L., M.A.D., K.M.M. and A.T. performed behavioural testing. A.T., B.P.B. and K.X. helped perform the pulldowns. S.M.D. and S.K.-A. performed the CSPG signalling experiments. Y.S., S.K.-A., S.L. and S.A.B. contributed to experimental design and figure preparation. B.T.L. and J.S. designed all studies, analysed the data and wrote the paper. All authors discussed and helped prepare the manuscript.

Author Information Reprints and permissions information is available at www.nature.com/reprints. Readers are welcome to comment on the online version of the paper. The authors declare competing financial interests: details are available in the online version of the paper. Correspondence and requests for materials should be addressed to J.S. (JXS10@case.edu).

METHODS

In vitro DRG culture

DRG and satellite glia dissociation and culture. DRGs were harvested as previously described⁹. Briefly, DRGs were dissected from adult female Sprague–Dawley rats (Harlan) and incubated in a solution of collagenase II (200 U ml⁻¹, Worthington Biochemical Corporation) and dispase II (2.5 U ml⁻¹, Roche Diagnostics) in Ca²⁺/Mg²⁺ free Hank's balanced salt solution (HBSS-CMF, Invitrogen). Cells were centrifuged at 1,000–2,000 r.p.m., washed and gently triturated in HBSS-CMF three times. Dissociated DRGs were then resuspended in Neurobasal-A media supplemented with B-27, Glutamax, and penicillin/streptomycin (Invitrogen). DRGs were plated in Delta-T dishes (Fisher) at a density of 800 cells cm⁻² or on coverslips at a density of 1,000 cells cm⁻².

Dish preparation and time-lapse microscopy. Delta-T-cell culture dishes were prepared as previously described³¹. Culture dishes were rinsed with sterile water and then coated with poly-L-lysine (0.1 mg ml⁻¹, Sigma-Aldrich) overnight at room temperature, rinsed with sterile water, and allowed to dry. Aggrecan spot gradients were formed by allowing 2 µl of aggrecan solution (2 mg ml⁻¹ in HBSS-CMF, Sigma-Aldrich) to dry onto the culture surface. The surface of the dish was bathed in laminin solution (10 µg ml⁻¹ in HBSS-CMF, Invitrogen) for 3 h at 37 °C. The laminin bath was subsequently removed and cells were plated without allowing the surface of the dish to dry. For conditions with laminin alone, the aggrecan spots were excluded from the protocol.

Prior to time-lapse imaging, adult neurons were incubated at 37 °C for 4–6 days in Neurobasal-A media with either vehicle (water) or 2.5 µM peptide. Neurobasal-A media with HEPES (50 µM, Sigma-Aldrich) and either vehicle or 2.5 µM peptide was added to the cultures before imaging in a heated stage apparatus. Time-lapse images were acquired every 30 s for at least 1.5 h with a Zeiss Axiovert 405M microscope using a heated ×100 oil-immersion objective. Growth cones that extended normal to the spot rim were chosen for analysis. We tracked and charted the behaviour of growth cones in our *in vitro* assay with Metamorph software. *n* = 19 laminin, 24 control, 24 ISP, 26 ISP. For delayed treatment, *n* = 14 ISP and ChABC.

PTP σ concentration quantification. High-magnification images of PTP σ expression (R&D Systems, 1:100) in growth cones, either motile on uniform substrates of laminin (5 µg ml⁻¹) or dystrophic within the CSPG gradient were analysed with ImageJ. Both the growth cone and axon were manually traced and the mean pixel intensity was calculated. All images were taken using identical settings.

CSPG gradient crossing assay. CSPG gradients were prepared as described previously⁹. Glass coverslips (1.6 mm, Fisher Scientific) coated with poly-L-lysine and nitrocellulose were spotted with a 2 µl solution of aggrecan (0.7 mg ml⁻¹) and laminin (5 µg ml⁻¹) in HBSS-CMF (4 spots per coverslip). After the spots were allowed to dry, the coverslips were incubated with laminin (5 µg ml⁻¹) in HBSS-CMF at 37 °C for 3 h. Dissociated DRG neurons were plated at a density of 1,000 cells cm⁻² in Neurobasal-A supplemented with B27, Glutamax and penicillin/streptomycin and incubated for 5 days at 37 °C. For peptide experiments, appropriate concentrations of peptide were added to the media at the time of plating. For ChABC experiments, 0.1 U ml⁻¹ ChABC (Seikagaku) was added to coverslips for 2 h after the laminin bath before cell plating.

At 5 days, cultures were fixed in 4% paraformaldehyde in PBS for 30 min. After several rinses in PBS, the coverslips were incubated in blocking solution (5% normal goat serum or normal donkey serum, 0.1% BSA, and with or without 0.1% Triton X-100 in PBS) for 1 h at room temperature and then incubated overnight at 4 °C in primary antibody. Anti-βIII-tubulin (1:500; Sigma-Aldrich), anti-CS56 (1:500; Sigma-Aldrich), anti-PTP σ (1:100, R&D systems), anti-GFP (1:500, Invitrogen), anti-S100 (1:1,000, Sigma-Aldrich), anti-GFAP (1:5,000, DAKO), anti-NgR (1:100, Millipore) and anti-LAR (1:100, Santa Cruz) were used as primary antibodies. Coverslips were rinsed several times in PBS and then incubated in the appropriate secondary antibody (Molecular Probes) overnight at 4 °C. Coverslips were rinsed with PBS again, and mounted on glass slides in Citifluor (Ted Pella) mounting medium. Specimens were examined using a Leitz Orthoplan 2 fluorescence microscope.

Wedge identification.

The intracellular domains of rat PTP σ (Protein Data Bank (PDB) accession 2FH7) and human LAR (PDB accession 1RPM) were visualized using UCSF Chimera 1.6.1. The wedge domains of human, rat and mouse PTP σ and PTP δ were identified by BLAST alignment with the known wedge domain of LAR¹⁴.

Peptide preparation. Peptides were synthesized commercially with C-terminal amidation (Genscript), and purity was assessed as >98% by mass spectrometry.

Lyophilized peptides were dissolved in sterile water and stored at –80 °C until use. Peptide sequences are as follows: ISP, NH₂-GRKKRRQRRCDMAEHLERLKA NDSLKLSQEYESI-NH₂; human ISP, NH₂-GRKKRRQRRCDMAEHLERLKA NDSLKLSQEYESI-NH₂; ISP no TAT, NH₂-DMAEHMERLKANDSLKLSQEYESI-NH₂; ILP, NH₂-GRKKRRQRRCDLADNIERLKANDGLKFSQEYESI-NH₂; IDP, NH₂-GRKKRRQRRCELADHIERLKANDNLKFSQEYESI-NH₂; IMP, NH₂-DL LQHITQMKCAEGYGFKEEYESGRKKRQRRNC-NH₂; scrambled ISP, NH₂-G

RKKRRQRRRCIREDDSLMLYALAQEKKESNMHES-NH₂; TAT, NH₂-GRKKRQRRRC-NH₂.

Quantification. All quantification was done blind. The number of βIII-tubulin-positive axons crossing the CSPG gradient (visualized using the CS56 antigen) was counted and divided by the total number of neuronal cell bodies contained within each gradient. Each gradient was counted as an individual data point. *n* = 112 control, 43 ChABC, 20 scrambled ISP, 57 ILP, 18 human ISP, 18 IDP, 16 IMP, 16 ISP no TAT, 16 TAT. For ISP, *n* (µm) = 16 (10), 16 (5), 34 (2.5), 49 (1.25), 27 (0.625, 0.25, 0.025, 0.0025).

For analysis of PTP σ concentration, PTP σ -stained neuronal growth cones and axons either entering the gradient or growing on uniform laminin were manually traced using ImageJ and the average pixel intensity was calculated.

Astrocyte preparation. Astrocytes were harvested from postnatal day 0/1 (P0/1) rat cortex as previously described³¹. Cortices were finely minced and treated with 0.5% trypsin in EDTA. Cells were plated in DMEM/F12 (Invitrogen) with 10% FBS (Sigma-Aldrich) and 2 mM Glutamax on T75 flasks coated with poly-L-lysine and shaken to remove non-adherent cells. Astrocytes were allowed to mature in culture for at least 4 weeks, and used within 2 weeks of maturity. Astrocytes were harvested with trypsin and plated at a density of 12,500 cells cm⁻².

Adhesion assay. Poly-L-lysine-coated glass coverslips were uniformly coated with a mixture of aggrecan (25 µg ml⁻¹) and laminin (1 µg ml⁻¹) for 3 h at 37 °C. DRG neurons were plated on coverslips (as described earlier) and incubated for 5 days at 37 °C. Cultures were then removed from the incubator and placed on a rotary shaker for 15 min at 80 r.p.m. Control coverslips were removed from the incubator, but not placed on the shaker. After shaking, the supernatants were immediately collected, centrifuged, re-suspended in 20 µl Neurobasal-A media, and placed on ice. The number of neurons released from each coverslip was counted with a haemocytometer. Coverslips were carefully fixed with 4% paraformaldehyde and stained for βIII-tubulin to visualize remaining neurons and axons (as described earlier). *n* = 28 control and ILP, 16 ISP.

DNA constructs and electroporation. mPTP σ in pECFP-N1 was a gift from A. M. Craig. Full-length mouse PTP σ with four fibronectin domains (BC052462) was subcloned into pEF1α-AcGFP1-N1 (Clontech) between NheI and HindIII. pEF1α-mPTP σ -AcGFP1-N1 was electroporated into adult DRG neurons with the Amaxa Rat Neuron Nucleofector Kit (Lonza) using the manufacturer's instructions.

PTP σ pulldown

Biotinylated peptide pulldown. For pulldown experiments, we used the Pierce Pull-Down Biotinylated Protein:Protein Interaction Kit (Thermo Scientific 21115). 100 µg ml⁻¹ of biotinylated-peptide (Genscript) was incubated overnight on an orbital shaker at 4 °C with streptavidin beads. After incubation, extra biotin was added and allowed to incubate overnight to ensure the binding of all streptavidin. After three washes with TBS, either recombinant GST-tagged PTP σ ICD (D1/D2 500 ng, Sigma, D1 500 ng, Abcam), spinal cord lysate from either wild-type or PTP σ -null mice, or brain lysate from an adult female Sprague–Dawley rat. Neural tissue was quickly extracted and flash frozen with liquid nitrogen. The tissue was homogenized in tissue homogenization buffer (20 mM Tris, 0.5 mM EDTA, 0.5 mM EGTA and 8% sucrose, pH 7.4) and 1:500 protease inhibitor cocktail (Abcam) on ice. The lysate was centrifuged at 13,000 r.p.m. for 20 min before addition to the beads. One-hundred and fifty microlitres of each lysate was added to the beads and allowed to incubate overnight at 4 °C. After three washes, beads were incubated with elution buffer for 10 min at room temperature. Beads were then centrifuged at 12,000 r.p.m. to collect eluted lysate.

SDS-PAGE and western blot. Thirty microlitres of the pulldown material with 4× Laemmli Buffer was boiled for 10 min at 100 °C and loaded into 7.5% TBX Mini-Protein Gels (Bio-Rad 456-1029) with Bio-Rad Precision Plus Protein Standard (Bio Rad 161-0374). The gel was run for about 1.5 h at 100 V in 1× Tris Glycine SDS Buffer. Gels were stained with Sypro Ruby Red (Sigma-Aldrich) to visualize proteins within the gel. Transfer occurred overnight at 15 V using a PVDF membrane. We blocked at least 2 h in 5% milk powder, 0.1% Tween-20 before overnight incubation with an antibody against GST (Cell Signaling), PTP σ ICD (1:100, Abnova), PTP σ ECD (1:1,000, Abcam), anti-NgR (1:500, Millipore) or anti-LAR (1:1,000, R&D Systems). We washed five times for 5 min in 1× PBS-0.1% Tween-20 before blocking overnight with a horseradish peroxidase (HRP)-conjugated secondary (1:1,000). The blot was developed using a chemiluminescence substrate (Thermo Sci) after five times five 1× PBS/0.1% Tween-20 washes. All experiments were repeated >3 times.

CSPG signalling

Plating SH-SY5Y cells on laminin and CSPG substrates. The SH-SY5Y neuronal cell line (ATCC) was grown in Hyclone Dulbecco's modified Eagle's high-glucose media (GE Healthcare Life Sciences, SH-30081.02) supplemented with 4 mM L-glutamine, 1 mM sodium pyruvate, 1% penicillin/streptomycin/neomycin (PSN) and 10% heat-inactivated fetal bovine serum (Invitrogen). SH-SY5Y cells were plated at an initial density of 12,000 cells cm⁻² onto tissue culture surfaces for

4 days under different conditions, including (1) laminin, (2) laminin plus CSPG, (3) laminin plus CSPGs pre-treated with ChABC, (4) laminin plus ISP in the media, (5) laminin plus CSPG plus ISP in the media. Tissue culture dishes were coated with laminin ($2 \mu\text{g ml}^{-1}$, Sigma, L2020) and/or CSPG ($15 \mu\text{g ml}^{-1}$, Millipore, cc117) for 3 h at room temperature. Of note, CSPGs used in this study contained a mixture of neurocan, phosphacan, versican and aggrecan. Where appropriate, ChABC (0.1 U ml^{-1} , Sigma, C3667-10UN) was added with laminin plus CSPG mixture to tissue culture surfaces for 1 h and incubated at 37°C during coating and before cell plating. In the ISP condition, cells were pre-treated with ISP ($2.5 \mu\text{M}$) for 30 min.

Immunoblotting. Cells were harvested from culture plates 4 days after cell plating and homogenized in RIPA buffer (Thermo Fisher) containing SigmaFast Protease Inhibitor (Sigma). A total of $30\text{--}50 \mu\text{g}$ protein was loaded into the gel and then transferred to a nitrocellulose membrane (Bio-Rad). The membranes were then blocked in 5% non-fat milk in Tween Tris buffered saline (TBST) for 1 h and incubated overnight at 4°C with P-p44/42 MAPK (Cell Signaling, Rabbit 1:500) diluted in the blocking solution. The membranes were washed and incubated with HRP-conjugated goat anti-rabbit antibodies (1:4,000, Biorad). Membranes were then incubated in ECL plus immunoblotting detection reagents (Thermo Scientific Pierce) according to the manufacturer's specifications. Blots were then stripped of their primary and secondary antibodies for 30 min in 0.2 M NaOH and re-probed with primary antibody p44/42 MAPK (Erk1/2) (Cell Signaling, Rabbit 1:1,000) overnight followed by incubation with secondary antibody and ECL.

Quantification. Immunoreactive bands were quantified using AlphaEaseFC (FluorChem, 8900). The ratio of phosphorylated (p)Erk1/2 to total (t)Erk1/2 for each condition was calculated. Data are reported as means \pm s.e.m., and $P \leq 0.05$ was considered significant. Statistical analyses of intensity measurements were tested by one-way ANOVA comparing conditions followed by post-hoc pairwise multiple-comparison testing by the Holm–Sidak method.

Animals and contusive SCI

Animals. Adult female Sprague–Dawley rats (225–250 g) were obtained from Harlan. All procedures were approved by the Institutional Animal Care and Use Committees. PTP σ -null mice were provided by M. Tremblay. All PTP σ -null experiments were performed in collaboration with Y. Shen.

Contusive SCI. Briefly, adult female Sprague–Dawley rats (230–250 g) were obtained from Harlan and acclimated to the animal resource centre, behaviour analysis chambers and handlers. Rats were injected intraperitoneally with ketamine (60 mg kg^{-1}) and xylazine (10 mg kg^{-1}). The musculature was cut from T7–T9 and the dorsal surface of T8 was exposed by laminectomy. The vertebral column was stabilized by clamping the T7 and T9 vertebral bodies with forceps fixed to the base of an Infinite Horizon Impact Device. The animals were situated on the platform, and the 2.5 mm stainless steel impactor tip was positioned over the midpoint of T8 and impacted with 250 kdyn force. The overlying musculature was closed using suture, the skin was closed using wound clips and the animals were treated with Marcaine at the incision site. The force/displacement graph was used to monitor impact consistency and any animals that exhibited an abnormal impact graph or greater than 10% deviation from 250 kdyn were immediately excluded from the study.

After surgery, pain was monitored and animals were treated with intramuscular buprenorphine at signs of discomfort. In addition, manual bladder expression was performed 2–3 times daily for 2–3 weeks until a voiding reflex returned and animals could leak urine. Five vehicle animals and two ILP animals were removed from the study and euthanized due to bladder infections and other serious ailments. One ISP-treated animal was removed due to a bladder stone.

Dorsal column crush injury. Dorsal column crush was performed similarly to as described previously³¹. Rats were anaesthetized with inhaled isoflurane gas (2%) for all surgical procedures. A T1 laminectomy was performed to expose the dorsal aspect of the C8 spinal cord segment. Durotomy was made bilaterally 0.75 mm from midline with a 30-gauge needle. A dorsal column crush lesion was then made by inserting Dumont no. 3 jeweller's forceps into the dorsal spinal cord at C8 to a depth of 1.0 mm and squeezing the forceps, holding pressure for 10 s and repeating two additional times. The muscle layers were sutured with 4-0 nylon suture, and the skin was closed with surgical staples. Animals were perfused at 14 days after injury.

Systemic peptide treatment. All randomization and peptide treatments were prepared by a blinded laboratory member not associated with behavioural analyses. First, a vehicle solution of 1.25 ml DMSO in 23.75 ml sterile saline was prepared for each animal. Next, appropriate peptide was added to each of the vehicle solutions where applicable so that the final peptide concentration of each solution was $5 \mu\text{M}$. Each drug solution was then aliquotted into 50 individual 1.5 ml Eppendorf tubes, each corresponding to a single animal's daily dose, and frozen at -20°C . All peptides were randomized and blinded to both the animal treatment administrator and separate behavioural analyser. At 24 h after SCI and each morning thereafter for 49 consecutive days, animals were given a $500 \mu\text{l}$ subcutaneous injection of the

appropriate blinded treatment into the back above the lesion ($n = 21$ vehicle, $n = 26$ ISP, $n = 10$ ILP). This experiment was carried out with five different cohorts of animals, with freshly synthesized peptide validated *in vitro* using the CSPG gradient assay and prepared for each cohort of animals. ILP treatments were only performed in the first and last cohort because we did not observe behavioural improvement with ILP treatment.

For the dose response, additional injured animals ($N = 5$ per group, cohort 4) were injected with $1/3 \times$ ISP ($3.6 \mu\text{g}$ per day), $1/2 \times$ ISP ($5.5 \mu\text{g}$ per day), $2 \times$ ISP ($22 \mu\text{g}$ per day), $3 \times$ ISP ($33 \mu\text{g}$ per day) or $4 \times$ ISP ($44 \mu\text{g}$ per day).

FITC-ISP peptide tracking. FITC-ISP was synthesized by Genscript with FITC conjugated to the N-terminus TAT domain. A single $500 \mu\text{l}$ injection of either $10 \mu\text{M}$ FITC-ISP in 5% DMSO plus saline or vehicle was given to animals subcutaneously into the back. At 1 h after injection, spinal cords were immediately removed and snap frozen. Twenty-micrometre-thick coronal sections of unfixed spinal cord tissue were collected on a cryostat and immediately imaged on a Leitz Orthoplan 2 fluorescence microscope.

Methysergide. A subset of ISP- and vehicle-treated animals were injected with methysergide (5 mg kg^{-1} , Sigma-Aldrich) intraperitoneally once a day for 3 days at 14 weeks after SCI ($n = 8$ vehicle, $n = 12$ ISP). Gridwalk and metabolic cage analyses were performed on days 0 and day 3, while BBB scoring was conducted daily. In addition to the full population, the animals whose behaviour started above or below a threshold level of two standard deviations above vehicle mean (see Fig. 4f) were plotted separately as responding and non-responding.

Behavioural analysis

Open field BBB. All behaviour analyses were conducted by two blinded observers separate from the researcher performing the daily dosing. Each animal was tested on days 1, 4, 7 and weekly thereafter until week 11. Animals were allowed to freely roam on an open field while being observed by two Ohio State Spinal Cord Injury Course expertly trained observers and scored according to the BBB guidelines²⁷. Any animal with a BBB score of greater than 1 at day 1 was removed from the study. Data were quantified as the average of the two hind limbs, compiled, and graphed.

Gridwalk. The gridwalk test was performed at 12 weeks after SCI. Animals were allowed to freely roam on a $75 \text{ cm} \times 40 \text{ cm}$ raised grid (2.5 mm thick wires, 2 cm gaps between wires) for 5 min while their progress was tracked with an overhead camera and quantified as total distance travelled (Ethovision). Foot faults were counted manually by a blinded observer and quantified as total number of hindlimb faults per metre.

Thermal hyperalgesia. Hyperalgesia analysis was performed at 12 weeks after injury by a blinded observer as published previously³². Animals were given 30 min to acclimate to the plexiglass cage before testing (Ugo Basile). The infrared radiation source (intensity = 58) was carefully placed under each hindpaw. Time to withdrawal was recorded as an average of five trials on each paw, with the longest and shortest time removed.

Mechanical allodynia. The Von Frey hair protocol for the hind paw was adapted from the Ohio State University Spinal Cord Injury Program. Briefly, animals satisfying the weight-bearing criteria were acclimated to the Von Frey testing boxes for at least 15 min. A total of ten trials were performed starting with the 5.18 monofilament while animals were distracted with a treat. The monofilament was tested on the plantar surface of the centre of the paw between the foot pads. A positive response was recorded if an animal withdrew its paw when the monofilament was presented. At least 30 s elapsed between each trial for the same hind paw. Positive responses led us to test with progressively smaller monofilaments. Conversely, negative responses led us to test with progressively larger monofilaments until monofilament 6.10. The threshold value was defined as the lowest monofilament level at which 50% or more of the trials resulted in a positive withdrawal.

Metabolic cage micturition analysis. At 6 weeks and 12 weeks after SCI, animals were placed in a metabolic cage (Braintree Scientific) for measurement of voiding patterns. The voided urine was measured continuously via a force transducer/strain gauge (Grass Technologies) and plotted in Spike2 (Cambridge Electrical Design, sampled at 20 Hz). Animals were kept in this cage for 16 h with ample water and food during the period of urine collection and measurement. The criteria for the micturition pattern analysis included void frequency (voids per h) and the void volume (ml per void). The total volume of expelled urine was not included because of variations in water intake between individual animals. $n = 11$ naive animals.

Urodynamics. Terminal urodynamic recordings were performed similarly to as described previously³³. Briefly, rats were anaesthetized at 14 weeks after SCI with 0.8 g kg^{-1} urethane delivered subcutaneously. A polyethylene-50 catheter was carefully inserted through the urethra into the bladder for delivery of saline. Fine wire electrodes ($76.2 \mu\text{m}$) ($0.003''$ diameter Teflon-insulated silver wire, A-M Systems) were inserted percutaneously via the vagina on both sides of the urethra to monitor the EUS electromyography (EMG) activity. The electrodes were connected to a preamplifier (HZP; Grass-Technologies), which was connected to an amplifier (Grass-Technologies) with low- and high-pass frequency filters at 30 Hz and 3 kHz,

respectively, and signal was sampled at a rate of 10 kHz (Power 1401, Spike2; Cambridge Electronic Design). Continuous cystometrograms (CMGs) were collected using constant infusion (6 ml h^{-1}) of room temperature saline (Aladdin-1000 single syringe infusion pump; World Precision Instruments) through the catheter into the bladder to elicit repetitive voids. The bladder pressure was recorded via the same catheter used for saline infusion, using a pressure transducer (Grass Technologies) connected to the recording system and sampled at a frequency of 2 kHz. Animals that received methysergide did not receive urodynamic analysis. $n = 11$ vehicle, 15 ISP, 6 ILP.

Immunocytochemistry and tracing

Perfusion and sectioning. To obtain spinal cord sections, rats were transcardially perfused with ice-cold 4% paraformaldehyde in PBS, and the spinal cords were dissected out. After the tissue was postfixed in 4% paraformaldehyde overnight at 4°C and cryoprotected with 30% sucrose, spinal cords were frozen in OCT mounting media and sectioned on a Hacker cryostat at a thickness of $20 \mu\text{m}$.

Immunocytochemistry. Mounted sections were washed three times with PBS followed by blocking in 5% normal goat serum (NGS) and 0.1% bovine serum albumin (BSA) in PBS. 0.1% Triton X-100 was added to the blocking buffer depending on the antigen used. After blocking, sections were incubated in primary antibody diluted in blocking buffer overnight at 4°C . Primary antibodies used were mouse anti-NeuN (1:100, Chemicon), anti-GFAP (1:1,000, Dako), mouse anti-ED1 (Chemicon, 1:100) rabbit anti-5-HT (1:500, Immunostar), and anti-neurofilament (1:500, Sigma-Aldrich). For *in vivo* PTP σ staining, sagittal $20 \mu\text{m}$ sections encompassing regions both rostral and caudal to the lesion were probed with anti-PTP σ antibody (1:500, Abnova). The next day, the sections were washed extensively with PBS and incubated in the appropriate secondary antibody or avidin substrate conjugated to AlexaFluor 488, 594 or 633 (1:500, Molecular Probes) overnight. After extensive washing, the sections were stained with DAPI (1:1,500 in PBS, Sigma-Aldrich), washed, coverslipped and viewed with a confocal microscope (Zeiss, Germany). Pixel intensity was measured on images taken on a standard fluorescent microscope (Leica) with a uniform exposure setting and analysed using ImageJ.

White matter analysis. Spared white matter analysis was conducted by EC staining as previously published³⁴. Briefly, room temperature $20 \mu\text{m}$ sections were placed in fresh acetone for 10 min, removed and allowed to dry for 30 min. Sections were stained with freshly filtered EC solution (Sigma-Aldrich) for 30 min and washed in running tap water for 5 min. The stain was differentiated in 5% ferric ammonium sulphate (Sigma-Aldrich) for 15 min and again washed with running tap water for 5 min. The differentiation was completed with borax-ferricyanide solution (Sigma-Aldrich) for 10 min, briefly washed with running tap water and allowed to dry. Slides were dehydrated in 70%, 95% and 100% ethanol for 2 min each followed by xylene for 2 min. Slides were coverslipped with a VectaMount Permanent Mounting Medium (Vector Laboratories). $n = 10$ vehicle, 14 ISP.

Lesion volume. Spinal cord sections stained with GFAP were analysed for lesion volume. After staining, sections were digitalized with a Leica SCN 400 Slide Scanner. Fifteen $20 \mu\text{m}$ coronal sections (one of every ten serial sections was stained, $200 \mu\text{m}$ between sections) both rostral and caudal of lesion epicentre were analysed for a total of 6 mm of spinal tissue. Sections were traced in ImageJ for volume calculation. $n = 9$ vehicle, 14 ISP.

5HT analyses. Coronal sections of lumbar spinal cord were analysed for 5HT intensity. The staining and imaging settings were uniform for all images. High exposure settings were used to maximize the signal to noise ratio, allowing for large patterns of 5HT expression to be visualized. ImageJ threshold analysis was used to eliminate all background from each section, leaving only the patterns of 5HT expression. The

area of innervation and per cent coverage of the grey matter was identified by analysing all particles in the grey matter at threshold intensity. Eight $20 \mu\text{m}$ sections, (corresponding to 1.6 mm of lumbar tissue) were analysed in ImageJ and averaged, with the highest and lowest intensity removed. $n = 13$ vehicle, 18 ISP.

Tracing. Cortical spinal tract labelling was performed as published previously³⁵. Ten per cent BDA (Molecular Probes) was injected into 16 locations in the rat motor cortex at 12 weeks after injury. Animals were killed 2 weeks after labelling. BDA labelling was visualized using an avidin-biotin-peroxidase incubation followed by diaminobenzidine and H_2O_2 (Vector Labs).

Statistical analysis. All statistical analyses were performed using Graphpad Prism. All results are presented as mean \pm s.e.m. Sample sizes were initially determined using statistical software to calculate the minimum total required number of animals or assays. All reported groups are above the minimum calculated sample size.

In vitro. For PTP σ intensity measurements, gradient crossings and adhesion assays, all statistical analysis was performed with one-way ANOVA between all groups in each individual experiment.

In vivo. For void frequency, void volume and gridwalk data sets, D'Agostino-Pearson and Shapiro-Wilk tests were first performed to determine if any individual data set abided to a normal, Gaussian distribution. Naive, vehicle control and ILP all passed the normality test, while ISP failed in all. Next, we performed ROUT analysis to identify outliers. No values were excluded from analysis, although a single ILP void frequency data point was identified as an outlier. Statistical analysis on these behaviours was performed with a one-way ANOVA and post-hoc Kruskal-Wallis test.

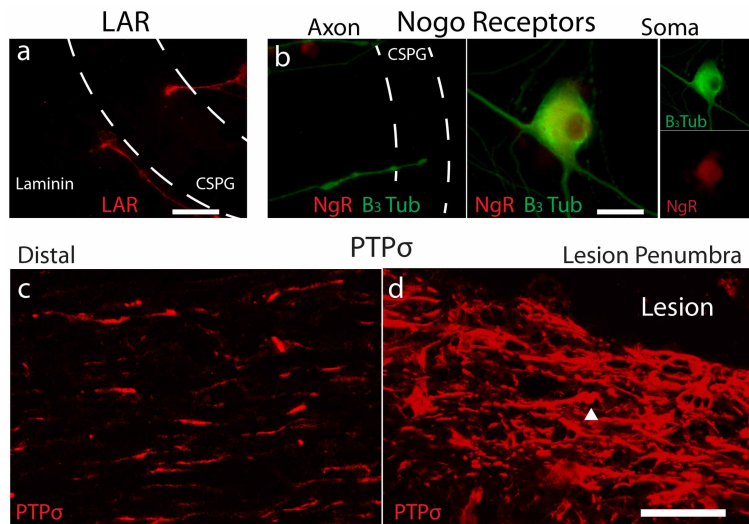
For BBB, we performed a repeated measures two-way ANOVA to compare vehicle, ILP and ISP. No normality tests were performed because BBB is a nonlinear scale. Post-hoc analysis at individual time point was performed with Tukey's test.

After methysergide treatment, BBB analysis was performed with repeated measures two-way ANOVA. For both gridwalk and void frequency, we compared pre-methysergide to post-methysergide treatment with a two-way ANOVA. The analysis between responding and non-responding animals was performed separately.

Anatomy. 5HT area and per cent grey matter coverage, the average value over the eight lumbar sections of ISP and vehicle control were compared with a Student's *t*-test.

Regression analysis. Regression analysis was performed by creation of a matrix of behavioural and anatomical scores for each animal. A separate matrix was created for vehicle and ISP treatment. Regression values (*r*) were identified by comparing two individual variables. The Pearson or Spearman coefficients were identified for parametric and non-parametric data sets, respectively.

31. Horn, K. P., Busch, S. A., Hawthorne, A. L., van Rooijen, N. & Silver, J. Another barrier to regeneration in the CNS: activated macrophages induce extensive retraction of dystrophic axons through direct physical interactions. *J. Neurosci.* **28**, 9330–9341 (2008).
32. Hargreaves, K., Dubner, R., Brown, F., Flores, C. & Joris, J. A new and sensitive method for measuring thermal nociception in cutaneous hyperalgesia. *Pain* **32**, 77–88 (1988).
33. Cheng, C. L. & de Groat, W. C. The role of capsaicin-sensitive afferent fibers in the lower urinary tract dysfunction induced by chronic spinal cord injury in rats. *Exp. Neurol.* **187**, 445–454 (2004).
34. Jakeman, L. B. in *Animal Models of Acute Neurological Injuries II* (eds Chen, J. Xu, X.-M. Xu, Z. C. & Zhang, J. H.) 417–442 (Springer, 2012).
35. Weidner, N., Ner, A., Salimi, N. & Tuszyński, M. H. Spontaneous corticospinal axonal plasticity and functional recovery after adult central nervous system injury. *Proc. Natl. Acad. Sci. USA* **98**, 3513–3518 (2001).

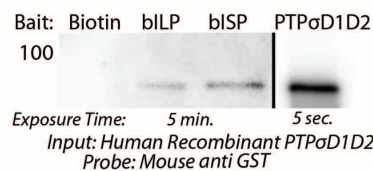
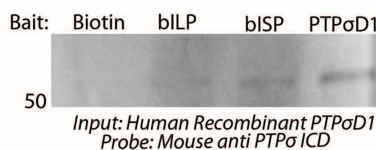
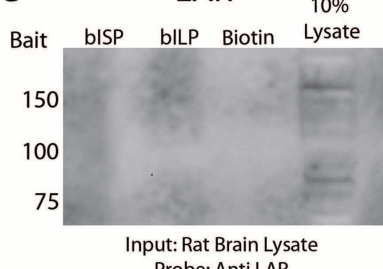
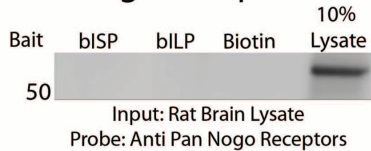


Extended Data Figure 1 | CSPG receptors LAR and NgR *in vitro* and PTP σ *in vivo*. **a**, LAR expression in motile (left, on laminin) and immobilized (right, within CSPG gradient) growth cones. **b**, Nogo receptors in a soma and

axons. Scale bars, 20 μm . **c, d**, PTP σ expression in the spinal cord 14 days after dorsal column crush injury. The arrowhead pointing upwards represents a labelled structure with dystrophic morphology. Scale bar, 50 μm .

a

PTPrF (LAR)	CAM27382 AAC37655 CAT14894	1316 ---GMRD-----HPPIPITDLADNIELKANDGLKFSQEYESIDPGQQFTWENSNSEVN	1366 Mouse
PTP σ	EDL38168 NP_062013 EAW69172	1325 ---GMLS-----HPPIPITDLADNIELKANDGLKFSQEYESIDPGQQFTWENSNLLEV	1375 Human
PTP δ	CAI24714 CAH70912	1321 ---GMAS-----HPPIPITDMAEHMERLKANDSLKLSQEYESIDPGQQFTWEHSNLEAN	1375 Mouse
PTP μ	NP_001098714	1330 ---GMAS-----HPPIPITELADHIERLKANDNLKFSQEYESIDPGQQFTWEHSNLEV	1331 Rat
		857 ETHTMASDTSSLVQSHTYKKREFADVPYQTQLHPAIRVADLQHITQMKCAEGYGKEEYESFEQGSAPWDASKDEN	1412 Human
			1371 Mouse
			1380 Human
			936 Human

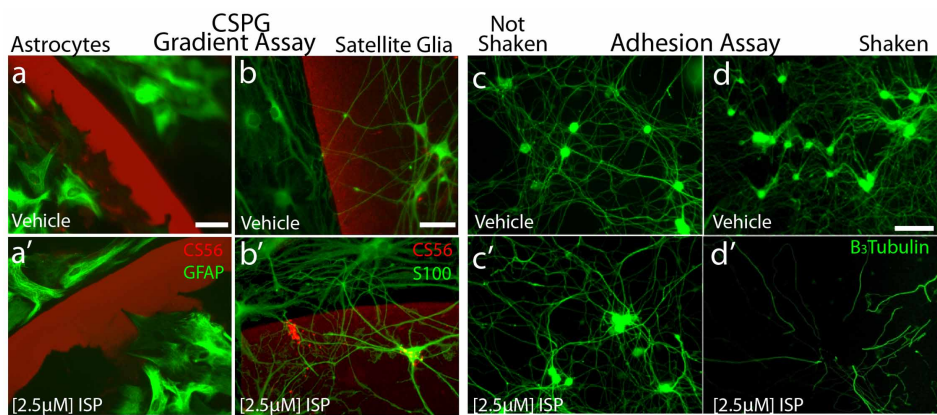
b Human LAR**c rHuman PTP σ ICD****d rHuman PTP σ ICD****e LAR****f Nogo Receptors**

Extended Data Figure 2 | LAR structure, sequence alignment and pulldown analysis. **a**, BLAST alignment of the known sequences of mouse, rat and human LAR, PTP σ , PTP δ and PTP μ . The wedge domain of each protein is aligned within the box. **b**, The tandem intracellular phosphatase domains of

human LAR with the previously characterized wedge domain (red)¹⁴.

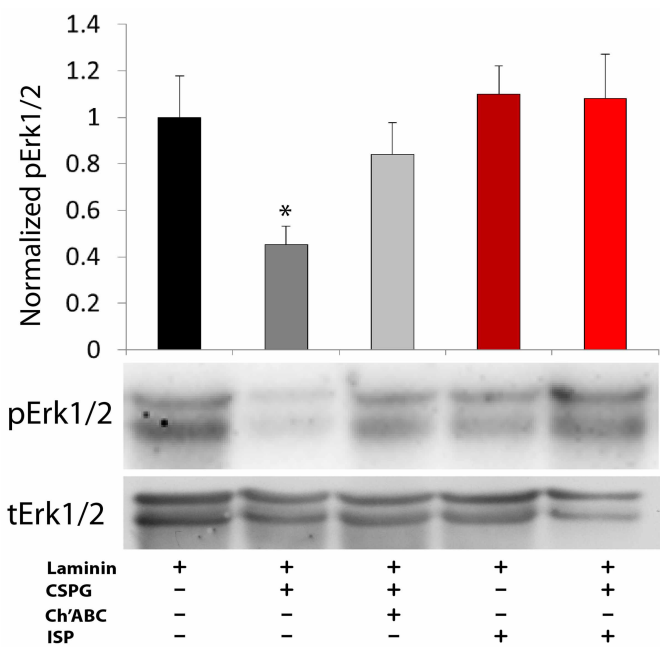
c, d, Pulldown of recombinant PTP σ with biotinylated (b)ISP or ILP.

e, f, Eluted lysate after pulldown was probed with antibodies against either LAR or pan-NgRs. Input is 10% lysate control.

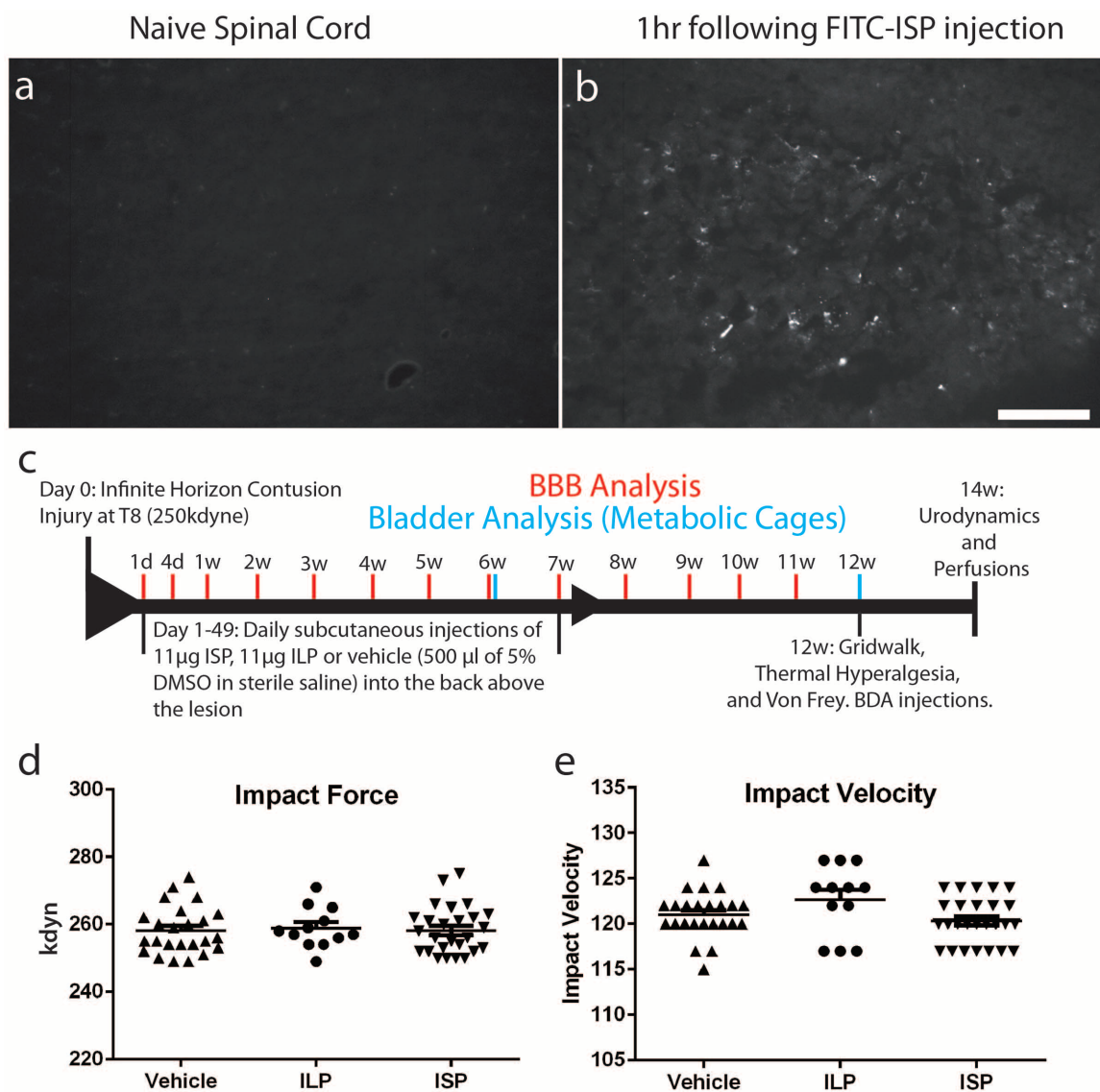


Extended Data Figure 3 | Astrocyte and satellite cell response to ISP and the adhesion assay. **a**, Purified GFAP-positive mature astrocytes (green) did not respond to ISP. **b**, S100-positive satellite glia were able to cross the gradient

of CSPG after ISP treatment. Scale bar, 50 μ m. **c, d**, Response of neurons and axons upon a CSPG-rich substrate to agitation after ISP treatment. Scale bar, 50 μ m.

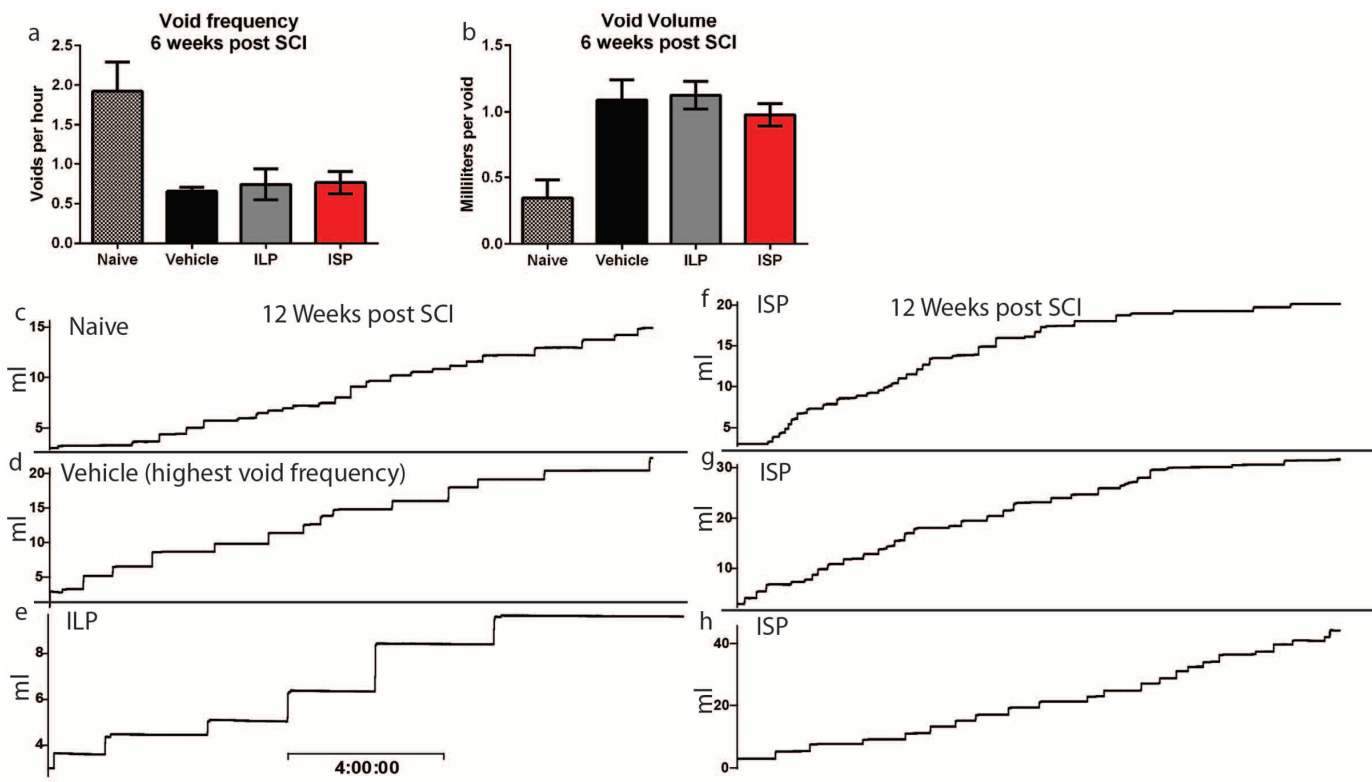


Extended Data Figure 4 | CSPG and ISP regulation of Erk1/2. Western blot analysis revealed a significant decrease in the phosphorylation ratio of Erk1/2 in SH-SY5Y cells plated on laminin ($2 \mu\text{g ml}^{-1}$) plus CSPGs ($15 \mu\text{g ml}^{-1}$) compared with laminin-only substrates, which was reversed by either pre-treatment with ChABC (0.1 U ml^{-1}) or 4 days of ISP treatment ($2.5 \mu\text{M}$). pErk1/2, phosphorylated Erk1/2; tErk1/2, total Erk1/2. Data normalized to laminin control. $N = 4$ independent experiments. * $P < 0.05$ versus all other conditions, one-way ANOVA, Tukey's post-hoc test.



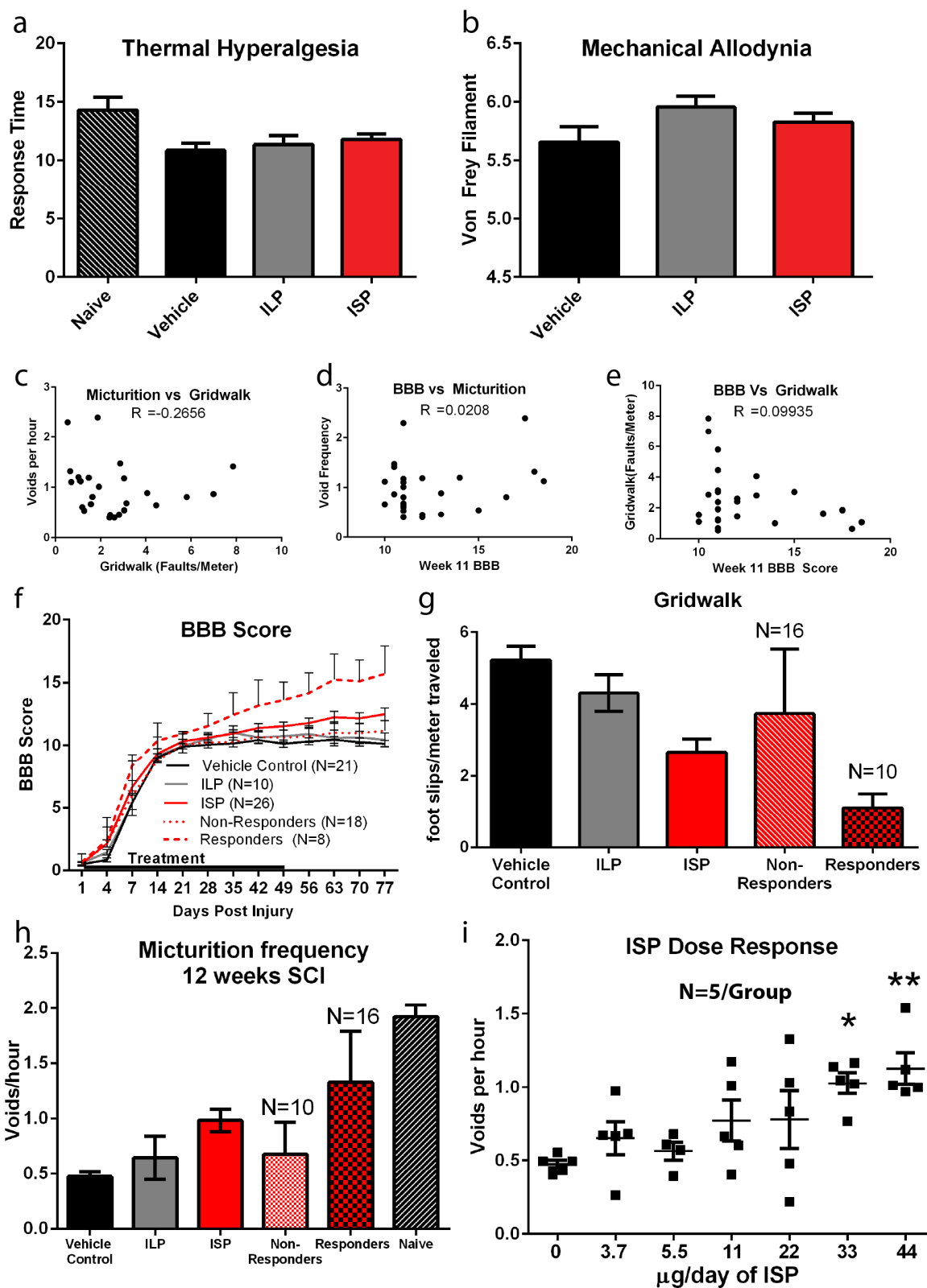
Extended Data Figure 5 | FITC-ISP *in vivo* and infinite horizon impaction.
a, b, Spinal cord 1 h after subcutaneous injections of FITC-ISP or vehicle. Scale bar, 100 μ M. **c,** Experimental design and timeline for *in vivo* experiment.

d, e, The force and impaction velocity of all animals that received an infinite horizon contusive injury. All impactions are within 10% from the target force of 250 kdyn, with an average force of 258.2 for both ISP and vehicle.



Extended Data Figure 6 | Metabolic cage analysis at 6 weeks after injury.
a, b, Void frequency and average void volume at 6 weeks after injury. $n = 11$ naive, 21 vehicle, 10 ILP and 26 ISP. c–h, Representative smoothed metabolic

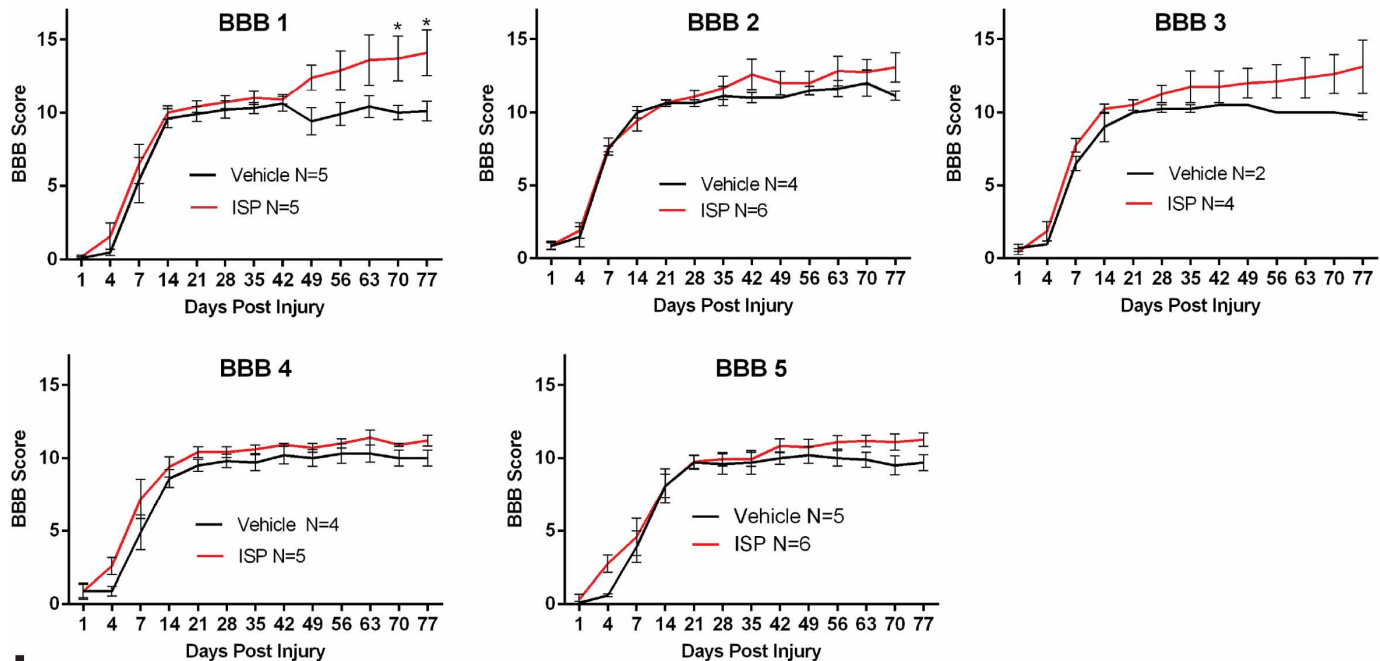
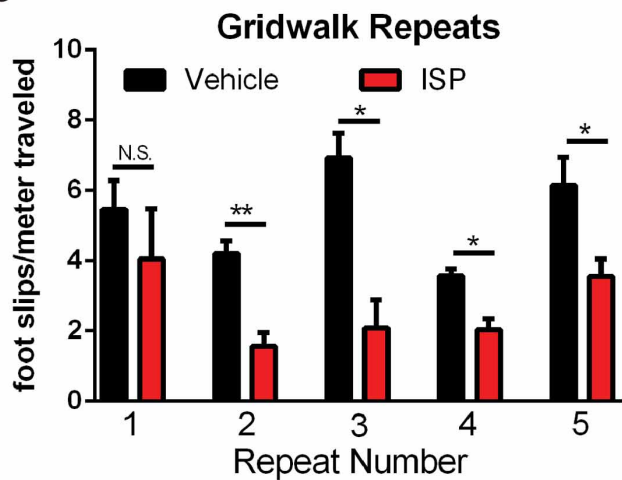
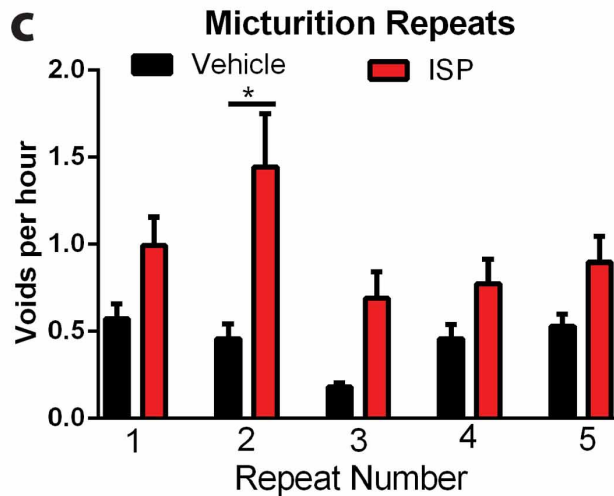
cage traces of a normal animal (c) and five treated animals (vehicle (d), ILP (e) and ISP (f, h) 12 weeks after injury. Void volume is plotted (in ml) as a function of time. Scale bar, 4 h.



Extended Data Figure 7 | Additional behavioural data and analyses.

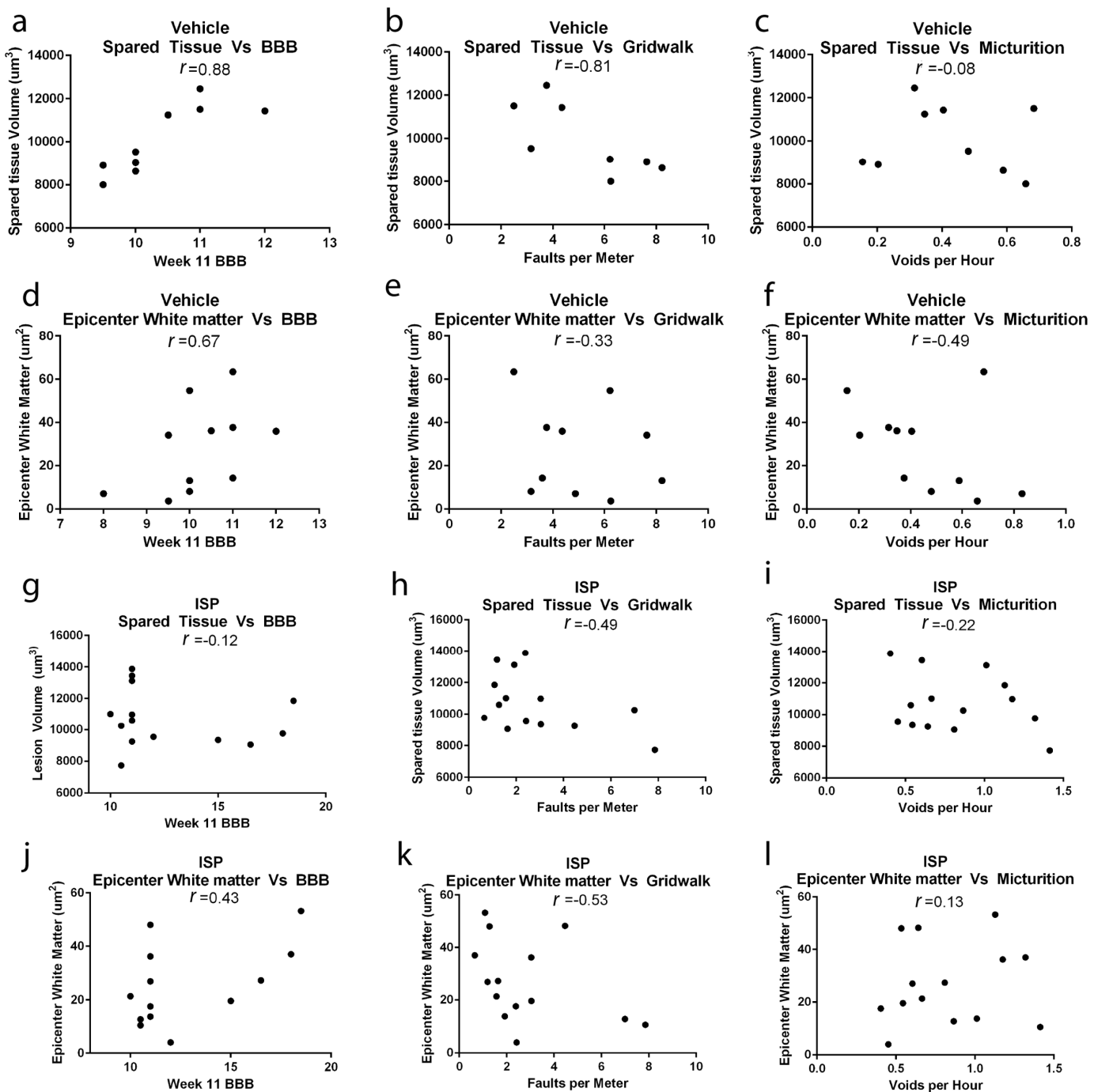
a, b, Average response to thermal (Hargrave's test) and mechanical (Von Frey test) stimuli at 12 weeks after injury ($n = 11$ naive, 21 vehicle, 10 ILP and 26 ISP for thermal, $n = 10$ vehicle, 4 ILP and 10 ISP for mechanical). **c–e**, Correlations between recovery of each individual motor behaviour in the ISP treatment group. **f–h**, For each behaviour, the ISP-treated animals that

recovered to two standard deviations relative to vehicle mean were separated and plotted as 'responders' while those that did not were plotted as 'non-responders'. The n for the responding and non-responding group for each behaviour is listed on the graph. **i**, An *in vivo* ISP dose–response plot in a single cohort of animals. A dose-dependent increase occurred in void frequency at 12 weeks after SCI.

a**b****c**

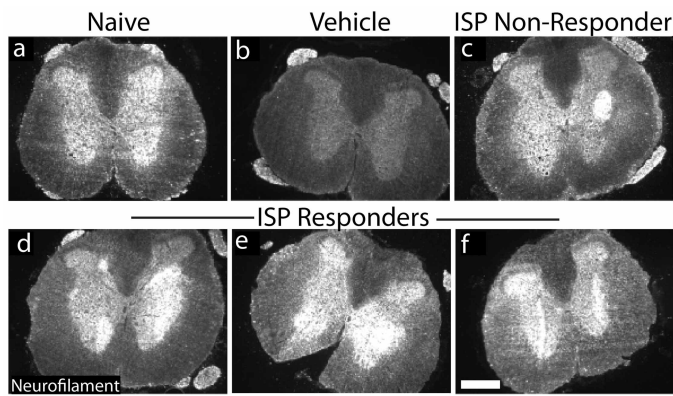
Extended Data Figure 8 | Five repetitions of *in vivo* experiments. a–c, The individual results of five repeats of *in vivo* experiments are plotted as individual cohorts of animals for BBB, gridwalk and void frequency. * $P < 0.05$, ** $P < 0.01$, repeated measures two-way ANOVA, Tukey's post-hoc test (BBB);

one-way ANOVA, Kruskal–Wallis post-hoc test (gridwalk and void frequency). Black indicates ISP versus control; red indicates ISP versus ILP. n for each condition is listed.



Extended Data Figure 9 | Correlation between spared tissue and behavioural recovery. a–l, Spared tissue volume (as measured by GFAP-positive tissue) or area of spared white matter at the epicentre (as measured by eriochrome cyanine staining) were plotted against behavioural scores for

vehicle- (a–f) and ISP-treated (g–l) animals. Pearson's correlation coefficient (r value) is reported for each comparison. Only animals whose spinal cord was processed and cut coronally were included in the analysis.

**Extended Data Figure 10 | Neurofilament staining at lumbar levels.**

a–f, Representative caudal neurofilament expression in lumbar spinal cord. Responders are ISP animals that demonstrated functional improvement (see Fig. 3n). All images were taken using identical settings. Scale bar, 500 μ m.